


Cite this: *RSC Pharm.*, 2024, **1**, 98

# Cerium oxide particles: coating with charged polysaccharides for limiting the aggregation state in biological media and potential application for antibiotic delivery†

Cléa Chesneau,<sup>a</sup> André Pawlak,<sup>b,c</sup> Séna Hamadi,<sup>a</sup> Eric Leroy<sup>a</sup> and Sabrina Belbekhouche  <sup>★a</sup>

Bacterial resistance to antibiotics has emerged as a major health issue. Developing new antibacterial systems is crucial. We propose to exploit cerium oxide particles which present interesting physico-chemical and biological properties. We demonstrated by zeta potential measurement that according to the pH, cerium oxide particles present either negatively or positively charged surfaces (isoelectric point determined around 8). We then take advantage of this property for modifying the particle surfaces with charged polysaccharides (dextran derivative to limit aggregation in aqueous media). The surface modification of particles has been examined by FT-IR, DRX and TGA measurements. The physicochemical properties of the resulting dispersion have been investigated as the size, dispersity and potential zeta value in physiological media. A fluorescent probe (Nile red) has then been loaded as a model of hydrophobic cargo, and then a hydrophobic antibiotic has been loaded (*e.g.* ciprofloxacin). Finally, the inhibitory effect on bacterial growth of the resulting antibiotic-loaded particles has been evaluated against antibiotic-resistant bacteria, namely spectinomycin-resistant *Escherichia coli*. These findings demonstrated the potential of the particles to be employed as an antimicrobial material, more specifically those resistant to antibiotic therapy.

Received 18th December 2023,  
Accepted 5th February 2024

DOI: 10.1039/d3pm00081h

rsc.li/RSCPharma

## 1. Introduction

Antibiotic use is often required to treat intracellular bacterial infections and resistance in pathogenic microbes, but because of their poor stability or water solubility, a step of vectorization is often needed for their efficient administration.<sup>1</sup> An efficient and safe antibiotic delivery system is needed for delivering therapeutic agents at an adequate concentration within the intracellular medium to prevent antibacterial resistance.<sup>2,3</sup>

Antibiotic-loaded particles provide a compelling alternative to antibiotics because they rely on entirely different mechanisms of antibacterial activity than those of antibiotics. The mode of action of particles is mainly based on direct contact with the wall of the bacterial cell, inducing damage to the bac-

terial cell.<sup>4</sup> In this sense, several works have reported on the increased antibacterial activity of antibiotic-conjugated particles.<sup>5–9</sup> Porous particles are highly appropriate materials for antibiotic delivery application. Among them, we may cite silica, calcium phosphate and calcium carbonate particles to name but a few.<sup>10</sup> For more insight into the fabrication of porous materials, the reader may refer to the recently published review articles.<sup>11,12</sup> Most of these particles can be safely excreted by the human body *via* the kidneys and can contain and then transport a high amount of therapeutic bioactives with few side effects.<sup>13</sup>

Among the different carriers, we focus on cerium oxide particles (CeO<sub>2</sub>) which are a rare earth oxide material employed in several technological applications.<sup>14</sup> In the last decade, cerium oxide particles have gained increased interest in the biomedical field, because of their self-regenerating antioxidant properties, *e.g.* are promising antioxidants for healing several untreatable oxidative-stress-related diseases, as discussed in previous works.<sup>15–17</sup> Cerium oxide nanoparticles certainly scavenge each ROS and RNS inclusive of the hydroxyl radical<sup>18</sup> and nitric oxide<sup>19</sup> whilst mimicking the antioxidant enzymes superoxide dismutase and catalase.<sup>20</sup> Interestingly, the antioxidant activity of such particles has been related to a shield-

<sup>a</sup> Université Paris Est Creteil, CNRS, Institut Chimie et Matériaux Paris Est, UMR 7182, 2 Rue Henri Dunant, 94320 Thiais, France.

E-mail: [sabrina.belbekhouche@cnrs.fr](mailto:sabrina.belbekhouche@cnrs.fr); Tel: + 331 4978 1149

<sup>b</sup> Institut National de la Santé et de la Recherche Médicale (INSERM), IMRB U955, Créteil, F-94010, France

<sup>c</sup> Univ Paris Est Creteil, Faculté de Médecine, UMRS 955, Créteil, F-94010 France

† Electronic supplementary information (ESI) available. See DOI: <https://doi.org/10.1039/d3pm00081h>



ing effect now not most effective on neurons,<sup>21</sup> but additionally on endothelial cells.<sup>22</sup> In this sense, cerium oxide nanoparticles had been evidenced to be useful for numerous pathologies which include most cancers,<sup>23</sup> cardiovascular injuries<sup>24</sup> or diseases of the principal worried system inclusive of Alzheimer's disease.<sup>25</sup>

A very important issue related to the application of nanoparticles in biological media is the need for a stable dispersion, especially at physiological pH. Unfortunately, cerium oxide particles are known to be prone to aggregation in aqueous media. In this sense, several pathways developed for stabilizing cerium oxide particles in aqueous media can be found in the literature.<sup>26,27</sup> For instance, Jiménez-Rojo *et al.* showed that lipid-based liposomes could stabilize suspensions of metal oxide nanoparticles.<sup>26</sup> Another promising approach is the stabilization of such particles by the adsorption of polyelectrolytes.<sup>28</sup> Polyelectrolytes are macromolecular chains consisting of linked charged or chargeable groups. The interactions of polyelectrolytes with particles have been examined in detail by Skirtach *et al.*<sup>29,30</sup> for example on a suspension of gold particles. They evidenced that polyelectrolytes can be efficiently used for improving the aggregation of gold nanoparticles.

Motivated by the aforementioned results, we decided to explore the interactions between ceria nanoparticles and an anionic polysaccharide to reduce the aggregation state. Polysaccharides are one of the biopolymer classes that are promising because of their weak toxicity toward mammalian cells.<sup>31</sup> Among them, we focus on dextran sulfate, selected herein because of its ability to retain its charge in a broad pH range.

Ciprofloxacin(1-cyclopropyl-6-fluoro-1,4-dihydro-4-oxo-7-(1-piperazinyl)-3-quinoline carboxylic acid) is a fluoroquinolone antibiotic classically employed to treat numerous bacterial infections such as lung infections.<sup>32</sup> Unfortunately, its potential benefits are limited by low bioavailability, poor water solubility ( $\geq 1 \text{ mg mL}^{-1}$  in water) and a short half-life. These shortcomings may be limited by administering the antibiotic through an alternative approach.

Research has been reported on the incorporation of ciprofloxacin into particles and their antibacterial activity has been evaluated.<sup>33–35</sup> Although many researchers have fabricated ciprofloxacin-loaded particles for different biomedical applications, to the best of our knowledge, cerium oxide particles have not been hitherto loaded with ciprofloxacin for use against spectinomycin-resistant *Escherichia coli* (which is an antibiotic-resistant bacteria). Therefore, in the present paper, cerium oxide particles loaded with ciprofloxacin have been fabricated towards this aim.

## 2. Materials and methods

### 2.1. Materials

Cerium oxide particles, dextran sulfate ( $\text{dex}^-$ ,  $M_n \sim 2.10^4 \text{ g mol}^{-1}$ ,  $D \sim 1.15$  determined by size exclusion chromatography;

see Fig. S1†), Nile red and ciprofloxacin were purchased from Sigma-Aldrich. Lysogeny broth (LB) culture medium was purchased from Fisher Scientific. Water at  $18 \text{ M}\Omega$  was produced using a Milli-Q system (Millipore).

### 2.2. Isoelectric point (pI) of cerium oxide particles suspended in aqueous media

The isoelectric point (pI) of the suspension of cerium oxide particles was determined by preparing a suspension of cerium oxide particles ( $0.1 \text{ g L}^{-1}$ ) at different pH values (ranging from 2 to 12). Each sample was analyzed in triplicate using a Zetasizer.

### 2.3. Coating of cerium oxide particles by negatively charged dextran

The surface modification of negatively charged cerium oxide particles was done *via* the saturation method. In the literature, this approach is widely described.<sup>36–38</sup> This elegant approach proposes the possibility of directly incorporating the required amount of polyelectrolyte to coat efficiently all cerium oxide particle surfaces and then does not require a purification process. The saturation concentration of dex- has to be empirically determined over zeta potential measurements. A suspension of positively charged cerium oxide particles ( $0.025 \text{ g L}^{-1}$  at pH 2) was progressively covered with a polyanion, namely dex- ( $10 \text{ g L}^{-1}$  solubilized in water). The adsorption process of this negatively charged biopolymer was monitored by zeta potential measurements. The detailed conditions of the preparation of the nanomaterial suspension will be determined and then discussed in the text.

### 2.4. Hydrophobic cargo-loaded cerium oxide particles: investigation of Nile red and ciprofloxacin

A hydrophobic solution (Nile red or ciprofloxacin) at a concentration of  $1 \text{ g L}^{-1}$  in ethanol was mixed with a suspension of cerium oxide particles and stirred for 24 h. The particles were then centrifuged and washed with ethanol to remove the free drug. This process was repeated twice. The loading with the fluorescent probe (Nile red) was examined with an optical fluorescence ZEISS microscope.

### 2.5. Characterization of cerium oxide particles

**2.5.1 Size and zeta potential measurements.** Zeta potential measurement was performed on a Zetasizer Nano-ZS (Malvern Instruments) to determine the pI of the cerium oxide suspension in aqueous media and to monitor the adsorption of dextran sulfate (Zetasizer 4700 Malvern Instruments, Brookhaven Instruments Corporation, USA). Different pH values were obtained by adding 0.1 M NaOH or HCl. The intensity–intensity time correction function was analyzed by the cumulative method. Each measurement was repeated several times. The mean value of the hydrodynamic diameter was calculated from the diffusion measurement using the Stokes–Einstein equation.<sup>39</sup> In all cases, the standard deviation was lower than 5%.



**2.5.2 Chemical characterization.** Fourier-transform infrared (FTIR) spectra were recorded between 4000 and 400  $\text{cm}^{-1}$  using a Bruker Tensor 27 spectrometer (Bruker Optik GmbH, Germany). The samples were placed on the crystal of the ATR accessory and 32 co-added scans at 4  $\text{cm}^{-1}$  resolution were taken for each sample. Thermogravimetric analysis (TGA) was carried out using a Setaram LabSys thermobalance in air at a temperature range of 30 to 800  $^{\circ}\text{C}$  and a heating rate of 20  $^{\circ}\text{C}$  per minute. Structural characterization was performed by X-ray diffraction (XRD) using a D8 advance diffractometer (Bruker, Champs sur Marne, France) (Cu  $\text{K}\alpha$  radiation). Data were recorded over a  $2\theta$  range from 5 to 80 $^{\circ}$  with a step of 0.02 $^{\circ}$  at an incident wavelength  $\lambda$  of 1.54056  $\text{\AA}$ .

**2.5.3 Microscopic observations.** The morphology of cerium oxide particles was examined using an optical fluorescence ZEISS microscope (LSM 700 Laser Scanning Microscope, Carl Zeiss, France) and a Transmission Electron Microscope (TEM, FEI Tecnai F20).

### 2.6. Bactericidal activity of cerium oxide particles loaded with ciprofloxacin

For investigating the bactericidal activity of cerium oxide particles loaded with ciprofloxacin, to 10.5 mL of suspension of spectinomycin-resistant *E. coli* (first grown at 37  $^{\circ}\text{C}$  for 24 h in lysogeny broth medium), 500  $\mu\text{L}$  (10  $\text{mg mL}^{-1}$ ) of the suspension of particles were added and then incubated at 37  $^{\circ}\text{C}$ . Water was used as a reference. Bacterial growth was followed periodically by reading the optical density of bacterial suspensions using a UV-visible spectrophotometer at 620 nm.

The percentage of bacterial growth inhibition was estimated using eqn (1):

$$I(\%) : \text{percentage of inhibition} \quad (1)$$

$$(I = 100 - ((\text{OD}_{\text{sample}}/\text{OD}_{\text{ref}}) \times 100))$$

$\text{OD}_{\text{ref}}$  and  $\text{OD}_{\text{sample}}$  correspond to the optical density (OD) of the reference (suspension of bacteria alone) and the sample (suspension of bacteria in which was added a suspension of ciprofloxacin-loaded cerium oxide particles), respectively.

### 2.7. Bacterial biofilm formation

A biofilm of *E. coli* was prepared on a polystyrene plate by using the protocol developed by Ashrit *et al.*<sup>40</sup> The bacterial viability was investigated *via* an orange acridine test coupled with fluorescence microscopy observation.<sup>41</sup>

## 3. Results and discussion

The investigated strategy relied on the use of cerium oxide particles for (i) limiting particle aggregation *via* a polysaccharide coating and (ii) hydrophobic antibiotic loading. The antibacterial activity of the designed materials was examined on environmental bacteria, namely antibiotic-resistant *Escherichia coli* (*E. coli*) in a liquid LB medium. Note that *E. coli* is a Gram-negative bacterium and is an important component of the

normal intestinal microflora of humans. However, it can be a highly versatile and frequently deadly pathogen.

### 3.1. Coating of cerium oxide particles by dextran sulfate: impact on aggregation in aqueous media

In Fig. 1, the DRX peaks are indexed using JCPDS card no: 34-0394. The DRX spectra of  $\text{CeO}_2$  nanoparticles indicated that the fine crystalline and single phase of  $\text{CeO}_2$  could be indexed to the cubic structure with the lattice parameters  $a = b = c = 5.411 \text{ \AA}$  and  $\alpha = \beta = \gamma = 90^{\circ}$ . Diffraction peaks were observed at 28.41 $^{\circ}$  (111), 32.99 $^{\circ}$  (200), 47.37 $^{\circ}$  (220), 56.26 $^{\circ}$  (311), 59.03 $^{\circ}$  (222), 69.27 $^{\circ}$  (400), 76.60 $^{\circ}$  (331) and 79.01 $^{\circ}$  (420). The broadened peak showed nanometer-sized crystallites. The average crystallite size ( $D$ ) of  $\text{CeO}_2$  nanoparticles has been estimated using the Debye-Scherrer equation (eqn (2)):

$$D = \frac{k\lambda}{\beta \cos \theta} \quad (2)$$

where  $\lambda$  is the wavelength of Cu- $\text{K}\alpha$  radiation,  $D$  is the crystallite size,  $k$  is a constant and its value is taken as 0.9,  $\theta$  is the diffraction angle and  $\beta$  is the full-width at half maximum (FWHM). The result obtained evidenced nanosized  $\text{CeO}_2$  particles in powder form (lower than 30 nm).

After drying a suspension of cerium oxide particles prepared at 0.5  $\text{g L}^{-1}$  in water at pH 6, images of such particles were obtained by Transmission Electron Microscopy. Fig. 2A clearly shows that pristine or “naked” cerium oxide particles present a high trend of aggregation in aqueous media. From TEM, we also notice the polydispersity, cuboidal shape and heterogeneity in particle characteristics. This result is difficult to explain as for this investigation, we use commercial powders with an unknown synthesis procedure. We supposed that the method used to prepare them does not take place in a controlled manner and leads to the observed characteristics.

One of the prerequisites for examining the adsorption behavior of polyelectrolytes on metal oxide aqueous surfaces is to

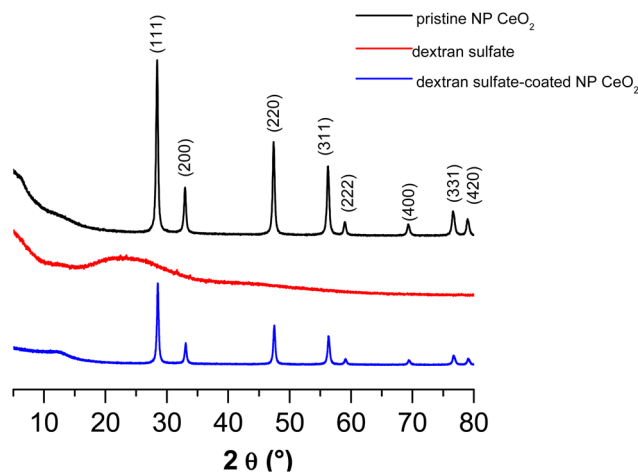


**Fig. 1** DRX spectra of pristine cerium oxide particles (—), dextran sulfate (—) and dextran sulfate-coated cerium oxide particles (—).



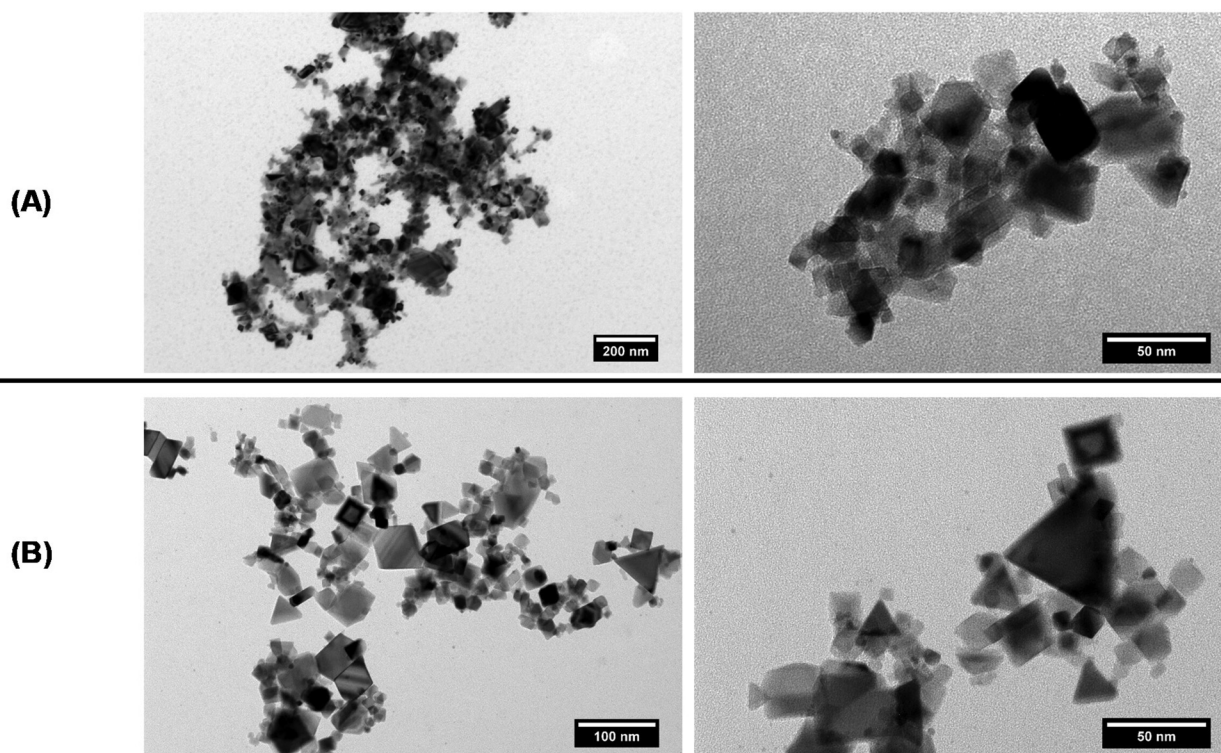


Fig. 2 TEM pictures of (A) pristine cerium oxide particles and (B) dextran sulfate-coated cerium oxide particles.

determine the isoelectric point (pI). This parameter was determined by measuring the zeta potential values of cerium oxide particle suspensions at  $0.025 \text{ g L}^{-1}$   $\text{CeO}_2$  particles and with various pH values between 2 and 11. The zeta potential values as a function of pH are presented in Fig. 3. From linear interp-

olation, an isoelectric point of 8.3 was derived. This is in accordance with the results obtained by the work by Quik *et al.*<sup>42</sup> and Van Hoecke *et al.*,<sup>43</sup> who determined an isoelectric point of 8.0 and 7.9 respectively, for the same nature particles. Therefore pristine particles may not be suitable for biological pH and thus this is the reason why we have developed our strategy, i.e. coating such particles with dextran sulfate.

With the aim of limiting the aggregation of cerium oxide particles in aqueous media, surface modification of the charged cerium oxide particle nanoparticles was performed by a direct saturation method. This means neither washing nor purification steps. Considering the surface modification of charged particles by polyelectrolytes, the centrifugation process is one of the most used methods to separate adsorbed polyelectrolytes onto the particle surfaces from free polyelectrolytes in solution. However, this presents some drawbacks; for instance, it is time-consuming. The saturation method is a more attractive strategy, as this offers the great advantage of avoiding post-processing procedures, e.g. washing and centrifugation steps. The amount of polyelectrolytes needed to be adsorbed onto the particles was experimentally estimated by zeta-potential measurements.<sup>38,44</sup>

As the ceria nanoparticles are positively charged at pH = 2 (see Fig. 3), and dextran sulfate is negatively charged (Fig. 4A) in the entire pH range, the coating of ceria nanoparticles is supposed to occur at pH 2. The addition of dextran sulfate to a suspension of  $\text{CeO}_2$  particles induces a decrease of the potential zeta value from a positive to a negative value confirming

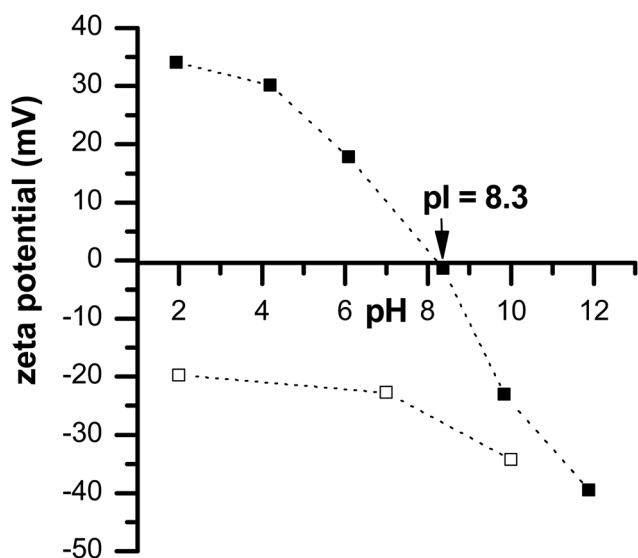


Fig. 3 Zeta potential values of a suspension of pristine  $\text{CeO}_2$  particles (■) and dextran sulfate-coated cerium oxide particles (□) as a function of pH in deionized water.



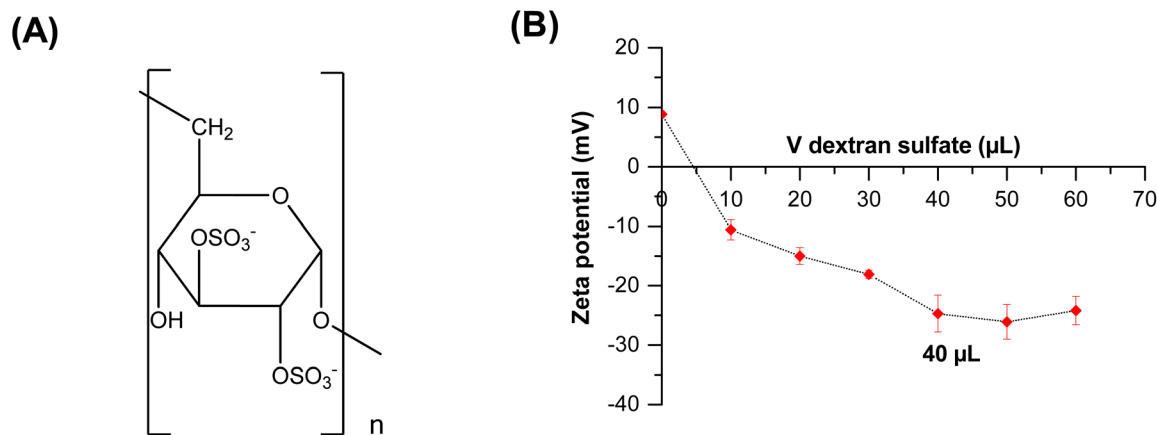


Fig. 4 (A) Chemical structure of dextran sulfate, (B) determination of the saturation concentration of dextran sulfate over zeta potential measurements.

the adsorption of this polyelectrolyte (in this case dex-) on the surface of metal oxide particles. The addition of dex- was stopped from the moment the measured zeta potential value of the suspension of the coated cerium oxide nanoparticles reached a value near to those obtained for the free dextran sulfate in solution (Fig. 4B). Thus, it can be supposed that the amount of free dextran sulfate in the suspension was very insignificant/low. The required volumes of stock dextran sulfate solution ( $10 \text{ g L}^{-1}$ ) to form a stable first layer were  $40 \mu\text{L}$  for cerium oxide particles.

As a first test, a visual observation (*i.e.* sedimentation test) of both dextran sulfate-coated and uncoated samples was done at various pH values. Sedimentation of uncoated  $\text{CeO}_2$  particles was observed at  $\text{pH} = 8$  (Fig. 5); this was not seen with the dextran derivative coating. This result proved that stability is increased by coating the cerium oxide particles with dextran sulfate and it also served as a clear indicator that dextran sulfate coating occurs. In contrast to pristine cerium oxide particles, dextran sulfate coated-cerium oxide particles remain

negatively charged regardless of the pH (see Fig. 3), and this ensures colloidal stability.

From Fig. 6, in the FTIR spectrum of dextran sulfate the presence of the sulpho group ( $\text{SO}_2$ ) can be determined by the presence of absorption bands at about  $1220 \text{ cm}^{-1}$  and  $979 \text{ cm}^{-1}$  assigned to  $\nu_{\text{as}}(\text{S}=\text{O})$  and  $\nu_{\text{s}}(\text{S}=\text{O})$  vibrations, respectively, as well as by the presence of absorption bands at  $804 \text{ cm}^{-1}$  and  $580 \text{ cm}^{-1}$  assigned to  $\nu_{\text{as}}(\text{O}-\text{S}-\text{O})$  and  $\nu_{\text{s}}(\text{O}-\text{S}-\text{O})$  vibrations, respectively.<sup>45</sup> The spectral region from  $1000$  to  $700 \text{ cm}^{-1}$  is important for the structural analysis of polysaccharides and is assigned to C-CH, C-C-O, O-C-O and C-O-C. The band around  $3470 \text{ cm}^{-1}$  is seen and can be assigned to the O-H group. For the FTIR spectrum of cerium oxide particles, a band around  $3460 \text{ cm}^{-1}$  is present, which can be assigned to the vibrational tension mode of O-H<sup>46</sup> due to residual water and/or hydroxyl groups. A small band at  $1040 \text{ cm}^{-1}$  is seen and may be attributed to the stretching vibrations of Ce-O-C.<sup>47</sup> The O-C-O stretching band is also seen in the region  $1300-1600 \text{ cm}^{-1}$ . The absorption band at

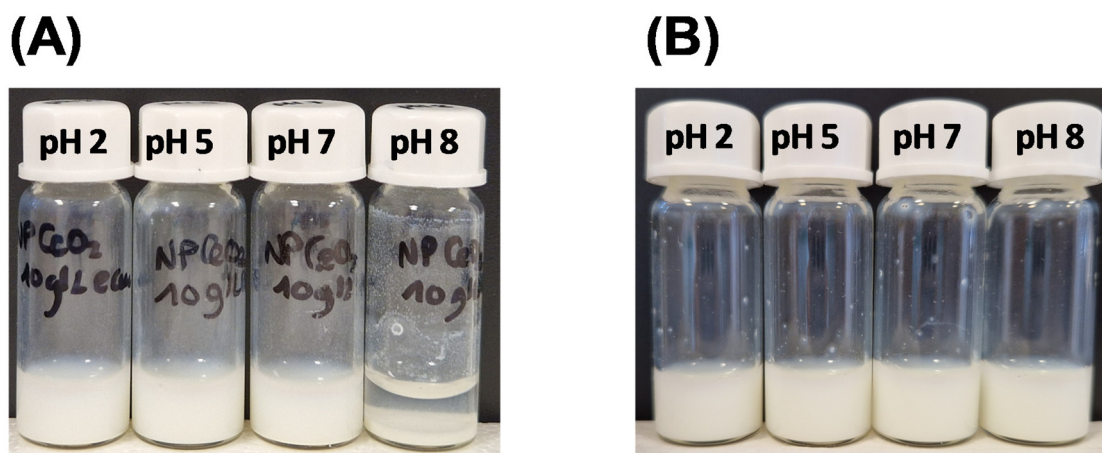
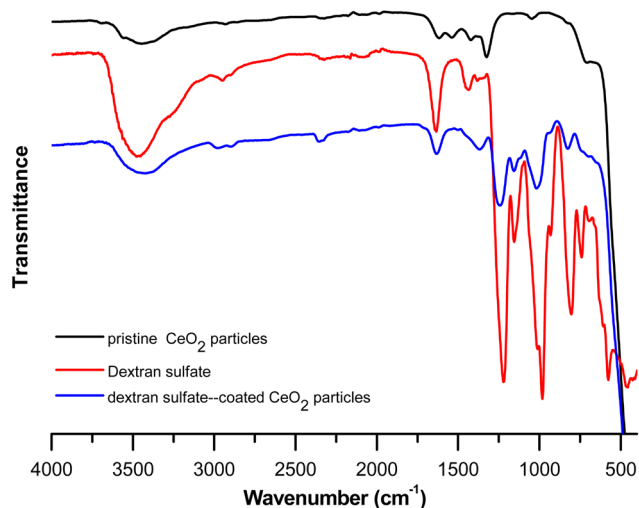


Fig. 5 (A) Solution of pristine  $\text{CeO}_2$  particles dispersed in water at pH 2, 5, 7 and 8 and (B) solution of dextran sulfate-coated  $\text{CeO}_2$  particles dispersed in water at pH 2, 5, 7 and 8.





**Fig. 6** Fourier Transform Infrared (FTIR) spectra of pristine cerium oxide particles (—), dextran sulfate (—) and dextran sulfate-coated cerium oxide particles (—).

around  $1630\text{ cm}^{-1}$  is assigned to the bending vibration of absorbed molecular water. The band at  $700\text{ cm}^{-1}$  can be assigned to Ce–O stretching. The FTIR spectrum of dextran sulfate-coated cerium oxide particles shows the characteristic peaks (cited below) of both dextran sulfate and cerium oxide particles.

In Fig. 1, the DRX spectrum of the dextran sulfate does not present any peak which is due to the amorphous structure of this polysaccharide. The DRX spectrum of dextran sulfate-coated cerium oxide particles presents the characteristic peak of pristine cerium oxide.

The influence of the size of the cerium oxide particles suspended at  $0.025\text{ g L}^{-1}$  in water at  $\text{pH} = 2$  was investigated. Table 1 shows sizes that vary from  $1189 \pm 64\text{ nm}$  to  $277 \pm 27\text{ nm}$  after dextran sulfate coating as well as a decrease in the polydispersity value (varies from 0.7 to 0.3). The dextran derivative coating allows for limiting the aggregation of cerium oxide particles and favors colloidal stability.

After drying a suspension of dextran sulfate-coated cerium oxide particles, the surface morphology of the obtained dextran sulfate-coated cerium oxide particles examined by transmission electron microscopy (TEM) is shown in Fig. 1B and reveals that the particles are less aggregated than without the coating. This result confirmed the DLS measurement reported in Table 1 and previously discussed.

**Table 1** DLS and zeta potential values for cerium oxide particles (pristine and coated with dextran sulfate) suspended at  $0.025\text{ g L}^{-1}$  in water at  $\text{pH} = 2$

	Pristine CeO <sub>2</sub> (pH 2)	Coated CeO <sub>2</sub> particles with dex- (pH 2)
Size (nm)	$1189 \pm 64$	$277 \pm 27$
Polydispersity	0.7	0.3

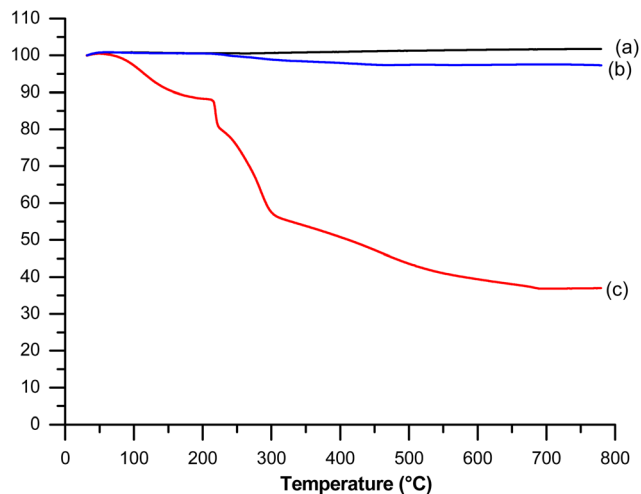


**Fig. 7** TGA curves of (a) pristine cerium oxide particles, (b) dextran sulfate-coated cerium oxide particles and (c) dextran sulfate.

Thermogravimetric analysis of cerium dioxide nanoparticles, dextran sulfate and dextran sulfate-coated particles are shown in Fig. 7. Dextran sulfate started to decompose at around  $100\text{ }^{\circ}\text{C}$  until  $700\text{ }^{\circ}\text{C}$  (weight loss 30%). CeO<sub>2</sub> particles show no significant weight loss which indicates good thermal stability. In contrast to pristine CeO<sub>2</sub> particles, dextran sulfate-coated CeO<sub>2</sub> particles present a weight loss of 5% in the temperature range studied which is in accordance with the dextran sulfate deposition of cerium oxide particles and the amount can then be estimated as 5% of dextran sulfate in the studied sample.

The experimental results obtained using multiple techniques confirm that adsorption of dextran sulfate takes place on the CeO<sub>2</sub> particle surface under examined experimental conditions and allows limiting aggregation of the metal oxide when suspended in aqueous media.

### 3.2. Antibiotic loading inside cerium oxide particles

Cerium oxide particles were selected because of their non-toxic nature at low concentrations.<sup>15,16</sup> Herein, we used commercial cerium oxide particles to load hydrophobic cargo.

**3.1.1. Proof-of-concept: loading of Nile red.** The Brunauer–Emmett–Teller (BET) method was applied to characterize pristine cerium oxide particles. It was found that the BET surface area is around  $54\text{ m}^2\text{ g}^{-1}$  and the total pore volume ( $\text{cm}^3\text{ g}^{-1}$ ) is  $0.16\text{ cm}^3\text{ g}^{-1}$ . As shown in Fig. 8, Nile red, a hydrophobic probe (water solubility lower than  $1\text{ g L}^{-1}$ ), was then successfully loaded inside cerium oxide particles. Pristine cerium oxide particles do not have any fluorescence characteristics. In contrast, for the Nile red-loaded cerium oxide particles, fluorescence has been observed and is characteristic of this fluorescent chemical (Fig. 8). This then clearly shows the entrapment of this hydrophobic cargo in the studied particles.

**3.1.2. Antibiotic loading: loading of ciprofloxacin.** In the human body, ciprofloxacin has a short active half-life and is practically insoluble in water. The vectorization of this anti-



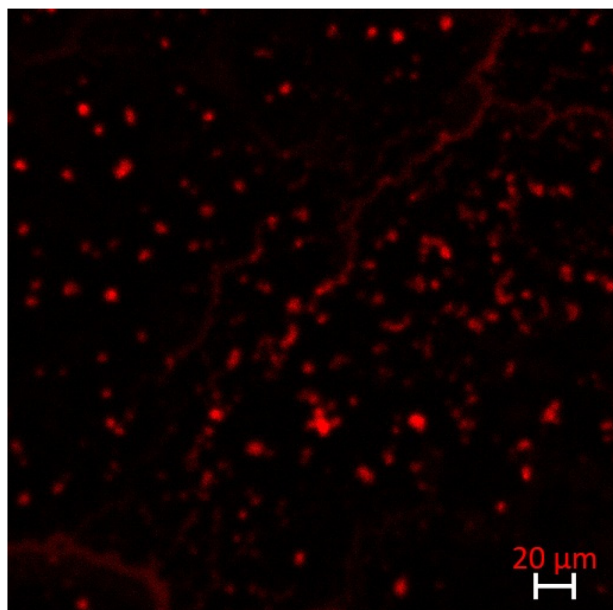


Fig. 8 Fluorescence image of Nile red-loaded cerium oxide particles.

biotic is thus of major interest for its loading and delivery to the site of infection. Moreover, it is important to take into account antibiotic resistance in bacteria. In this context, we evaluated the use of cerium oxide particles for the antibiotic loading and subsequent release.

Loading was done by soaking cerium oxide particles into hydrophobic antibiotic solutions under the same conditions found for the loading of the hydrophobic Nile Red. The antibiotic remains loaded inside the particle for up to 15 days which significantly extends the persistence ability of ciprofloxacin.

In Fig. 9, the growth curves of *E. coli* were determined based on the bacterial cell optical density. We distinguished two classical phases of growth: the exponential phase and the stationary phase.<sup>48</sup> The stepwise variation in the growth rate could be assigned to the changes seen in expression profiles of genes coding for enzymes involved in biosynthesis or nutrient assimilation.<sup>49</sup> In the microbial growth curve, the growth phases can also be defined in terms of the metabolic processes and physiological states occurring during growth, which have been directly correlated with the nutritional content of the growth media.<sup>50</sup> Fig. 9 presents the bacterial growth response according to exposure to the antibiotic-loaded particles over time. Bacterial growth was strongly impacted in the presence of cerium oxide particles loaded with ciprofloxacin. Indeed, the exposition of such particles to bacteria led to the direct inhibition of their growth (inhibition of up to 94%). This is of major interest as ciprofloxacin is almost insoluble in water and bacterial resistance to this antibiotic has emerged.<sup>51</sup> For instance, Fantin *et al.* reported that increasing the concentration of this antibiotic induced a better bactericidal effect but induced resistance to ciprofloxacin in human commensal bacteria.<sup>51</sup>

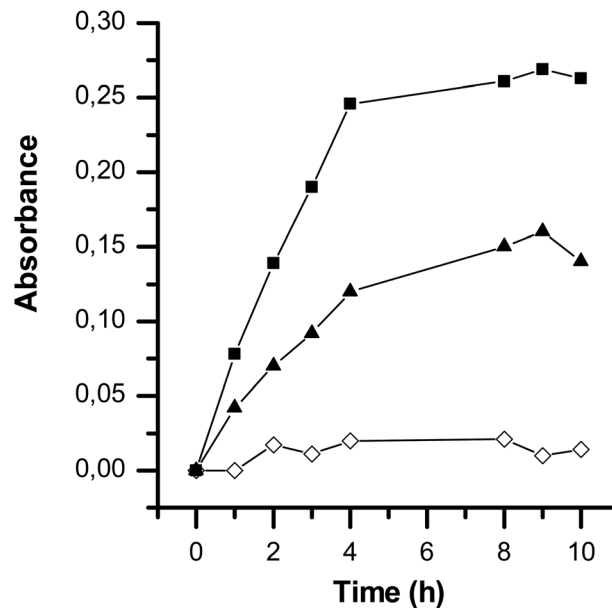


Fig. 9 Growth study of spectinomycin-resistant *E. coli* in LB medium in water ■, in the presence of cerium oxide particles loaded with ciprofloxacin (◇), and in the presence of a solution of ciprofloxacin at  $0.07 \mu\text{g ml}^{-1}$  (▲).

The MIC value of ciprofloxacin is reported to be around  $0.15\text{--}4 \mu\text{g ml}^{-1}$  against *S. aureus* and *E. coli*.<sup>52,53</sup> The required amount of ciprofloxacin was then directly released when using ciprofloxacin-loaded cerium oxide particles.

On the other hand, as seen in Fig. 9, the addition of a solution of ciprofloxacin in the presence of the bacteria studied induced partial inhibition of the activity of this bacterium. This is due to the hydrophobicity of ciprofloxacin, which does not enter the bacteria sufficiently at this concentration. This clearly highlights the importance of vectoring this antibiotic into the particles studied.

Ciprofloxacin is an antibiotic that is known to be a DNA-targeting agent, and to interact with their target type II topoisomerases to enhance the generation of single- and double-strand DNA breaks associated with stalled or collapsed replication forks.<sup>54,55</sup> The cerium oxide particles loaded with this antibiotic may first interact with bacterial surfaces. Then, the antibiotic is released, which causes bacterial cell wall damage.

Note that we can combine the two approaches proposed in this work to generate a  $\text{CeO}_2$  delivery system with high solubility. Indeed, we have shown that after trapping the compound (part developed in section 3.2), it is still possible to modify the surface with the polyelectrolyte (part developed in section 3.1). These particles were then brought into contact with an *E. coli* biofilm prepared on the surface of a polystyrene plate. Polystyrene plates were selected as these materials are currently employed in medical materials which are embedded in the human body and microbial strains easily adhere to these materials and then form biofilms.<sup>56</sup> We show that compared to the uncoated particles those coated with dextran enhance their



incorporation in the biofilm and induce bacterial death due to antibiotic release. Indeed, bacterial viability was examined with acridine orange which allows discriminating between dead or living bacteria.<sup>57</sup> A red fluorescence was observed after staining bacteria (Fig. SI 2<sup>†</sup>), showing the death of bacterial cells due to exposure to dextran-coated particles.

## 4. Conclusion

We demonstrated (from TEM, DLS, electrophoretic mobility, FTIR and TGA measurements) that the adsorption of dextran sulfate on a suspension of ceria nanoparticles takes place under the examined experimental conditions. Under studied physicochemical conditions, after the adsorption of the biopolymer, the aggregation is limited in aqueous media.

We then reported on the use of cerium oxide particles as good candidates for designing antibacterial systems loaded with a hydrophobic antibiotic namely ciprofloxacin (poor water solubility,  $\geq 1$  mg mL<sup>-1</sup> in water). Our approach is simple and allows us to tackle the issue of poor solubility in aqueous media. The particles could be loaded with a sufficient amount of antibiotics to prevent the growth of spectinomycin-resistant *E. coli*. We showed that antibiotic-loaded particles were more effective than the antibiotic alone.

We then combined surface modification with a dextran derivative and antibiotic loading. We demonstrated the effectiveness of such a system on an *E. coli* biofilm prepared on the surface of a polystyrene plate. This plate has been selected as these materials are currently employed in medical materials which are embedded in the human body and microbial strains easily adhere to these materials and then form biofilms.

## Conflicts of interest

There are no conflicts to declare.

## Acknowledgements

We gratefully acknowledge the Agence Nationale de la Recherche (grants ANR-22-CE92-0086) for the financial support during this research project.

## References

- G. L. Mislin and I. J. Schalk, Siderophore-dependent iron uptake systems as gates for antibiotic Trojan horse strategies against *Pseudomonas aeruginosa*, *Metalomics*, 2014, **6**(3), 408–420.
- D. Zhao, R.-X. Zhuo and S.-X. Cheng, Modification of calcium carbonate based gene and drug delivery systems by a cell-penetrating peptide, *Mol. BioSyst.*, 2012, **8**(12), 3288–3294.
- R. Y. Pelgrift and A. J. Friedman, Nanotechnology as a therapeutic tool to combat microbial resistance, *Adv. Drug Delivery Rev.*, 2013, **65**(13–14), 1803–1815.
- L. Wang, C. Hu and L. Shao, The antimicrobial activity of nanoparticles: present situation and prospects for the future, *Int. J. Nanomed.*, 2017, **12**, 1227.
- V. Akbari, *et al.*, Ciprofloxacin nano-niosomes for targeting intracellular infections: an in vitro evaluation, *J. Nanopart. Res.*, 2013, **15**(4), 1556.
- S. Chono, *et al.*, Pharmacokinetic and pharmacodynamic efficacy of intrapulmonary administration of ciprofloxacin for the treatment of respiratory infections, *Drug Metab. Pharmacokinet.*, 2007, **22**(2), 88–95.
- H. X. Ong, *et al.*, Liposomal nanoparticles control the uptake of ciprofloxacin across respiratory epithelia, *Pharm. Res.*, 2012, **29**(12), 3335–3346.
- L. Michely, *et al.*, Easy way for fabricating calcium carbonate hybrid microparticles-supported carrier: Focus on the loading of several hydrosoluble cargos all at once, *J. Drug Delivery Sci. Technol.*, 2022, **74**, 103485.
- F. A. Said, *et al.*, Antibiotic loading and development of antibacterial capsules by using porous CaCO<sub>3</sub> microparticles as starting material, *Int. J. Pharm.*, 2020, **579**, 119175.
- W. Wang, *et al.*, Calcium carbonate-doxorubicin@ silica-indocyanine green nanospheres with photo-triggered drug delivery enhance cell killing in drug-resistant breast cancer cells, *Nano Res.*, 2018, **11**(6), 3385–3395.
- X. Du, *et al.*, Disulfide-bridged organosilica frameworks: designed, synthesis, redox-triggered biodegradation, and nanobiomedical applications, *Adv. Funct. Mater.*, 2018, **28**(26), 1707325.
- Y. Li and J. Shi, Hollow-structured mesoporous materials: chemical synthesis, functionalization and applications, *Adv. Mater.*, 2014, **26**(20), 3176–3205.
- J. G. Croissant, *et al.*, Syntheses and applications of periodic mesoporous organosilica nanoparticles, *Nanoscale*, 2015, **7**(48), 20318–20334.
- C. Sun, H. Li and L. Chen, Nanostructured ceria-based materials: synthesis, properties, and applications, *Energy Environ. Sci.*, 2012, **5**(9), 8475–8505.
- I. Celardo, E. Traversa and L. Ghibelli, Cerium oxide nanoparticles: a promise for applications in therapy, *J. Exp. Ther. Oncol.*, 2011, **9**(1), 47–51.
- S. Das, *et al.*, Cerium oxide nanoparticles: applications and prospects in nanomedicine, *Nanomedicine*, 2013, **8**(9), 1483–1508.
- F. Caputo, M. De Nicola and L. Ghibelli, Pharmacological potential of bioactive engineered nanomaterials, *Biochem. Pharmacol.*, 2014, **92**(1), 112–130.
- Y. Xue, *et al.*, Direct Evidence for Hydroxyl Radical Scavenging Activity of Cerium Oxide Nanoparticles, *J. Phys. Chem. C*, 2011, **115**(11), 4433–4438.
- J. M. Dowding, *et al.*, Cerium oxide nanoparticles scavenge nitric oxide radical (<sup>•</sup>NO), *Chem. Commun.*, 2012, **48**(40), 4896–4898.





- 20 V. Baldim and N. Yadav, Polymer-Coated Cerium Oxide Nanoparticles as Oxidoreductase-like Catalysts, *ACS Appl. Mater. Interfaces*, 2020, **12**(37), 42056–42066.
- 21 S. Nagarajan, *et al.*, Novel biocompatible electrospun gelatin fiber mats with antibiotic drug delivery properties, *J. Mater. Chem. B*, 2016, **4**(6), 1134–1141.
- 22 Q. Bao, *et al.*, Simultaneous Blood-Brain Barrier Crossing and Protection for Stroke Treatment Based on Edaravone-Loaded Ceria Nanoparticles, *ACS Nano*, 2018, **12**(7), 6794–6805.
- 23 H. Ghaznavi, *et al.*, Neuro-protective effects of cerium and yttrium oxide nanoparticles on high glucose-induced oxidative stress and apoptosis in undifferentiated PC12 cells, *Neurol. Res.*, 2015, **37**(7), 624–632.
- 24 F. Pagliari, *et al.*, Cerium oxide nanoparticles protect cardiac progenitor cells from oxidative stress, *ACS Nano*, 2012, **6**(5), 3767–3775.
- 25 C.-C. Yu, *et al.*, Electrospun scaffolds composing of alginate, chitosan, collagen and hydroxyapatite for applying in bone tissue engineering, *Mater. Lett.*, 2013, **93**, 133–136.
- 26 N. Jiménez-Rojo, *et al.*, Lipidic nanovesicles stabilize suspensions of metal oxide nanoparticles, *Chem. Phys. Lipids*, 2015, **191**, 84–90.
- 27 E. J. Salazar-Sandoval, M. K. G. Johansson and A. Ahniyaz, Aminopolycarboxylic acids as a versatile tool to stabilize ceria nanoparticles – a fundamental model experimentally demonstrated, *RSC Adv.*, 2014, **4**(18), 9048–9055.
- 28 D. I. Gittins and F. Caruso, Tailoring the Polyelectrolyte Coating of Metal Nanoparticles, *J. Phys. Chem. B*, 2001, **105**(29), 6846–6852.
- 29 A. G. Skirtach, *et al.*, Nanoparticles Distribution Control by Polymers: Aggregates versus Nonaggregates, *J. Phys. Chem. C*, 2007, **111**(2), 555–564.
- 30 B. V. Parakhonskiy, *et al.*, Nanoparticles on Polyelectrolytes at Low Concentration: Controlling Concentration and Size, *J. Phys. Chem. C*, 2010, **114**(5), 1996–2002.
- 31 S. Tokura, *et al.*, *Biological activities of biodegradable polysaccharide*, in *Macromolecular symposia*, 1996, Wiley Online Library.
- 32 B. Scully, *et al.*, Ciprofloxacin therapy in cystic fibrosis, *Am. J. Med.*, 1987, **82**(4A), 196–201.
- 33 A. Toncheva, *et al.*, Antibacterial fluoroquinolone antibiotic-containing fibrous materials from poly(L-lactide-co-D,L-lactide) prepared by electrospinning, *Eur. J. Pharm. Sci.*, 2012, **47**(4), 642–651.
- 34 A. R. Unnithan, *et al.*, Wound-dressing materials with antibacterial activity from electrospun polyurethane-dextran nanofiber mats containing ciprofloxacin HCl, *Carbohydr. Polym.*, 2012, **90**(4), 1786–1793.
- 35 S. P. Parwe, *et al.* Synthesis of ciprofloxacin-conjugated poly (L-lactic acid) polymer for nanofiber fabrication and antibacterial evaluation, *Int. J. Nanomed.*, 2014, **9**, 1463–1477, DOI: [10.2147/ijn.s54971](https://doi.org/10.2147/ijn.s54971).
- 36 U. Bazylińska, *et al.*, Novel approach to long sustained multilayer nanocapsules: influence of surfactant head groups and polyelectrolyte layer number on the release of hydrophobic compounds, *Soft Matter*, 2011, **7**(13), 6113–6124.
- 37 U. Bazylińska, *et al.*, Influence of dicephalic ionic surfactant interactions with oppositely charged polyelectrolyte upon the in vitro dye release from oil core nanocapsules, *Bioelectrochemistry*, 2012, **87**, 147–153.
- 38 S. Belbekhouche, *et al.*, Latex nanoparticles surface modified via the layer-by-layer technique for two drugs loading, *Colloids Surf., A*, 2017, **524**, 28–34.
- 39 T. Misono, Dynamic Light Scattering (DLS), in *Measurement Techniques and Practices of Colloid and Interface Phenomena*, ed. M. Abe, Springer Singapore, Singapore, 2019, pp. 65–69.
- 40 P. Ashrit, *et al.*, A microplate-based Response Surface Methodology model for growth optimization and biofilm formation on polystyrene polymeric material in a *Candida albicans* and *Escherichia coli* co-culture, *Polym. Adv. Technol.*, 2022, **33**(9), 2872–2885.
- 41 L. Boulos, *et al.*, LIVE/DEAD® BacLight™: application of a new rapid staining method for direct enumeration of viable and total bacteria in drinking water, *J. Microbiol. Methods*, 1999, **37**(1), 77–86.
- 42 J. T. K. Quik, *et al.*, Effect of natural organic matter on cerium dioxide nanoparticles settling in model fresh water, *Chemosphere*, 2010, **81**(6), 711–715.
- 43 K. Van Hoecke, *et al.*, Aggregation and ecotoxicity of CeO<sub>2</sub> nanoparticles in synthetic and natural waters with variable pH, organic matter concentration and ionic strength, *Environ. Pollut.*, 2011, **159**(4), 970–976.
- 44 A. Voigt, *et al.*, Membrane filtration for microencapsulation and microcapsules fabrication by layer-by-layer polyelectrolyte adsorption, *Ind. Eng. Chem. Res.*, 1999, **38**(10), 4037–4043.
- 45 M. Cakić, *et al.*, Synthesis, characterization and antimicrobial activity of dextran sulphate stabilized silver nanoparticles, *J. Mol. Struct.*, 2016, **1110**, 156–161.
- 46 S. Phoka, *et al.*, Synthesis, structural and optical properties of CeO<sub>2</sub> nanoparticles synthesized by a simple polyvinyl pyrrolidone (PVP) solution route, *Mater. Chem. Phys.*, 2009, **115**(1), 423–428.
- 47 D. Andreescu, E. Matijević and D. V. Goia, Formation of uniform colloidal ceria in polyol, *Colloids Surf., A*, 2006, **291**(1), 93–100.
- 48 B. L. Wanner and M. R. Wilmes-Riesenberg, Involvement of phosphotransacetylase, acetate kinase, and acetyl phosphate synthesis in control of the phosphate regulon in *Escherichia coli*, *J. Bacteriol.*, 1992, **174**(7), 2124–2130.
- 49 M. V. Baev, *et al.*, Growth of *Escherichia coli* MG1655 on LB medium: monitoring utilization of sugars, alcohols, and organic acids with transcriptional microarrays, *Appl. Microbiol. Biotechnol.*, 2006, **71**(3), 310–316.
- 50 G. Sezonov, D. Joseleau-Petit and R. D'Ari, *Escherichia coli* physiology in Luria-Bertani broth, *J. Bacteriol.*, 2007, **189**(23), 8746–8749.



- 51 B. Fantin, *et al.*, Ciprofloxacin dosage and emergence of resistance in human commensal bacteria, *J. Infect. Dis.*, 2009, **200**(3), 390–398.
- 52 A. K. Kidsley, *et al.*, Antimicrobial Susceptibility of *Escherichia coli* and *Salmonella* spp. Isolates From Healthy Pigs in Australia: Results of a Pilot National Survey, *Front. Microbiol.*, 2018, **9**(1207), DOI: [10.3389/fmicb.2018.01207](https://doi.org/10.3389/fmicb.2018.01207).
- 53 J.-P. Didier, *et al.*, Impact of ciprofloxacin exposure on *Staphylococcus aureus* genomic alterations linked with emergence of rifampin resistance, *Antimicrob. Agents Chemother.*, 2011, **55**(5), 1946–1952.
- 54 K. Drlica, *et al.*, Quinolone-mediated bacterial death, *Antimicrob. Agents Chemother.*, 2008, **52**(2), 385–392.
- 55 M. Malik, X. Zhao and K. Drlica, Lethal fragmentation of bacterial chromosomes mediated by DNA gyrase and quinolones, *Mol. Microbiol.*, 2006, **61**(3), 810–825.
- 56 A. Festas, A. Ramos and J. P. Davim, Medical devices biomaterials – A review, *Proc. Inst. Mech. Eng., Part L*, 2019, **234**, 146442071988245.
- 57 D. E. Francisco, R. A. Mah and A. C. Rabin, Acridine orange-epifluorescence technique for counting bacteria in natural waters, *Trans. Am. Microsc. Soc.*, 1973, 416–421.

